ACS Photonics

Article

pubs.acs.org/journal/apchd5

High-Modulation-Efficiency, Integrated Waveguide Modulator−Laser Diode at 448 nm

Chao Shen,[†] Tien Khee Ng,[†] John T. Leonard,[‡] Arash Pourhashemi,[‡] Hassan M. Oubei,[†] Mohd S. Alias,[†] Shuji Nakamura,[‡] Steven P. DenBaars,[‡] James S. Speck,[‡] Ahmed Y. Alyamani,[§] Munir M. Eldesouki,[§] and Boon S. Ooi*[,†]

[†]Photonics Laboratory, King Abdullah University of Science and Technology, Thuwal 21534, Saudi Arabia

[‡]Materials Department, University of California Santa Barbara, Santa Barbara, California 93106, United States

[§]King Abdulaziz City for Science and Technology (KACST), Riyadh 11442, Saudi Arabia

ABSTRACT: To date, solid-state lighting (SSL), visible light communication (VLC), and optical clock generation functionalities in the blue-green color regime have been demonstrated based on discrete devices, including light-emitting diodes, laser diodes, and transverse-transmission modulators. This work presents the first integrated waveguide modulator−laser diode (IWM-LD) at 448 nm, offering the advantages of small footprint, high speed, and low power consumption. A high modulation efficiency of 2.68 dB/V, deriving from a large extinction ratio of 9.4 dB and a low operating voltage range of 3.5 V, was measured. The electroabsorption characteristics revealed that the modulation effect, as observed from the red-shifting of the absorption edge, resulted from the external-field-induced quantum-confined Stark effect. A comparative analysis of the photocurrent versus wavelength spectra in semipolar- and polar-plane InGaN/GaN quantum wells (QWs) confirmed that the IWM−LD based on semipolar $(20\bar{2}1)$ QWs was able to operate in a manner similar to other III−V materials typically used in optical telecommunications, due to the reduced piezoelectric field. Utilizing the integrated modulator, a −3 dB bandwidth of ∼1 GHz was measured, and a data rate of 1 Gbit/s was demonstrated using on−off keying modulation. Our experimental investigation highlighted the advantage of implementing the IWM−LD on the same semipolar QW epitaxy in enabling a high-efficiency platform for SSL−VLC dual functionalities.

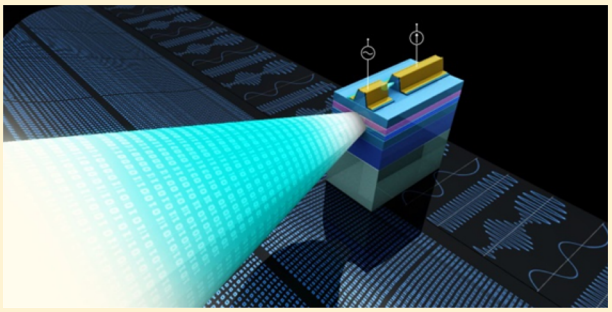

KEYWORDS: *laser diode, electroabsorption modulator, nitride semiconductor, solid-state lighting, visible light communication*

InGaN/GaN quantum well (QW)-based light-emitting diodes (LEDs) and laser diodes (LDs) are fundamental components of solid-state lighting (SSL).[1−4] The eventual widespread usage of such emitters is expected to usher in prospects of functional diversification into visible light communication (VLC), which has recently attracted increasing attention.[5−7] To date, LDs have been used in the VLC systems based on direct current modulation[6,8] for implementing signal modulation schemes, such as non-return-to-zero on−off keying (NRZ-OOK)[8] and orthogonal-frequency division multiplexing (OFDM).[7] Because blue emitters (λ = 440−460 nm) are widely accepted as fundamental components for white light communications,[7] it is anticipated that there will be a growing demand for a blue-emitting integrated waveguide modulator−laser diode (IWM−LD), which has a small footprint and a low power consumption, as well as multifunctionality by nature. Thus far, visible light modulators, either broadband or narrowband, were implemented using transverse-transmission modulators based on novel low-dimensional materials,[9] ZnSe-based QWs,[10] and III-nitrides, including InGaN/GaN QW,[11,12] GaN/AlGaN QW,[11,13] and GaN bulk film.[13] However, the integration of a waveguide electroabsorption (EA) modulator with a laser diode in the blue-green regime remains unexamined. The lack of interest in this effort originates from the fundamental issues of large spontaneous and piezoelectric polarization fields in *c*-plane InGaN/GaN QWs. As a result, it requires a large bias to offset the internal field, on the order of MV/cm,[14] making it highly inefficient compared to the phosphide- and arsenide-based counterparts.[15,16] In this work, we investigate the utilization of InGaN/GaN QWs on semipolar bulk GaN substrates for achieving an effective and efficient IWM−LD due to the reduced polarization fields in semipolar $(20\bar{2}1)$ InGaN/GaN QWs.[17−19] In our IWM−LD, a high modulation efficiency of 2.68 dB/V was derived from a large extinction ratio of 9.4 dB and a low operating voltage range of 3.5 V. Our approach based on the integration of optical waveguide modulators with laser diodes aimed to alleviate the drawbacks associated with direct modulation of the whole LDs, including the transient heating effect[13] and RC

Received: October 19, 2015
Published: January 25, 2016

DOI: 10.1021/acsphotonics.5b00599
ACS Photonics 2016, 3, 262−268

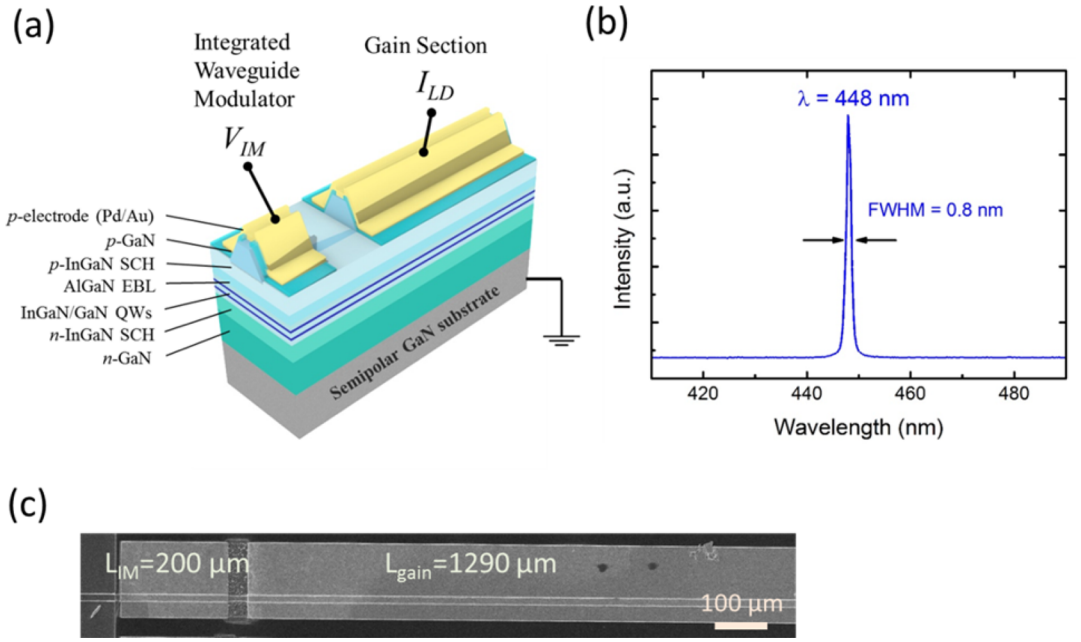

Figure 1. (a) Schematic of the structure of the IWM−LD. (b) Optical emission spectra of the IWM−LD showing a peak emission wavelength of 448 nm and a full-width at half-maximum (fwhm) of 0.8 nm. (c) SEM plane view of the fabricated multisection laser diode with an integrated modulator.

delay. A −3 dB bandwidth of 1 GHz was measured from the IWM−LD. For proof-of-concept demonstration, 1 Gbit/s data transmission using IWM−LD was also presented via an NRZ-OOK modulation scheme having a pseudorandom binary sequence (PRBS) 2^{10}-1 data stream. The advent of the SSL−VLC dual-function lamp utilizing our integrated EA modulation approach is amenable to the realization of energy-efficient, compact device architecture based on the efficient manipulation of a quantum-confined Stark effect (QCSE)-induced change in light absorption in semipolar InGaN/GaN quantum wells.

EXPERIMENTAL DETAILS

The InGaN/GaN MQW laser diode epi-structure was grown on semipolar $(20\bar{2}1)$ substrates provided by Mitsubishi Chemical Corporation using the metal−organic chemical vapor deposition technique. The epitaxial structure (Figure 1a) consisted of a 2 μm Si-doped n-GaN template, a 60 nm Si-doped n-$In_{0.05}Ga_{0.95}N$ separate confinement heterostructure (SCH) waveguiding layer, a four-period undoped multiple quantum well active region with 3.6 nm wide $In_{0.2}Ga_{0.8}N$ QWs and 7.5 nm wide GaN barriers, a 18 nm Mg-doped p-$Al_{0.15}Ga_{0.85}N$ electron blocking layer (EBL), a 60 nm low-Mg-doped p-$In_{0.05}Ga_{0.95}N$ SCH waveguiding layer ($[Mg] = 7.5 \times 10^{17}$ cm^{-3}), a 400 nm standard Mg-doped p-GaN cladding layer ($[Mg] = 1.5 \times 10^{18}$ cm^{-3}), and a 12 nm highly Mg-doped p-GaN contact layer ($[Mg] = 1 \times 10^{20}$ cm^{-3}). The ridge waveguide multisection laser diode was defined using UV photolithography and inductively coupled plasma etching. The isolation trench between the integrated modulator (IM) region and gain region is 10 μm wide and was etched into the InGaN cladding layer. The etching of the isolation trench is carefully controlled; the metal contact layer and highly doped GaN layer were removed, providing good electrical isolation and maintaining optical coupling. Facets were dry etched along the *a*-direction without dielectric coatings. Pd/Au and Ti/Al/Ti/Au metalization layers were deposited using sputter as p- and n-electrodes, respectively.

The optical power vs current (L−I) relations were measured using a Keithley 2520 laser diode test system with a calibrated Si photodetector and integrated sphere. The device was mounted on a homemade probe station with thermoelectric cooling. A Keithley 2400 source meter was used to provide dc modulation bias in the electrotransmission measurement. The setup also included an Ocean Optics HR 4000 high-resolution spectrometer, a halogen lamp, a 20× objective lens, and dc probes. In the photocurrent measurement, a halogen lamp, monochromator, power meter, and set of optics were used. With regard to the bandwidth and data transmission characterizations, the device was probed in the same setup, the gain section was probed by a set of dc probes, and the modulator section was probed by a set of rf probes. The ac small-signal modulation bandwidth measurement setup consisted of an Agilent E8361C PNA network analyzer, Picosecond Pulse Laboratories 5543 bias tee, and Menlo Systems APD 210 high-speed Si avalanche photodetector. An Agilent J-BERT N4903B bit error rate tester, an Agilent DCA-86100C digital communication analyzer, and a Picosecond Pulse Laboratories 5865 broadband amplifier were used in the NRZ-OOK data transmission setup.

RESULTS AND DISCUSSION

The studied multisection EA modulator−integrated laser diode is a three-terminal device consisting of a reverse-biased waveguide modulator section and a forward-biased gain section (Figure 1a). The device was grown on a semipolar $(20\bar{2}1)$ plane, which resulted in high-efficiency blue light emitters.[20,21] The IWM−LD is made of a 2 μm wide ridge waveguide to achieve single-mode lasing at 448 nm (Figure 1b). Each fabricated device consists of a 200 μm long IM section and a 1.29 mm long gain section. Both sections share the same QW active region layer structure and are optically coupled, allowing the emitted beam from the gain section to be modulated by the IM. It is noted that in InGaAs−InGaAsP-based devices additional band-gap change induced by annealing is required

DOI: 10.1021/acsphotonics.5b00599
ACS Photonics 2016, 3, 262−268

to achieve multiple sections with different transition energy levels to reduce absorption loss.[22] In the group III nitride, however, the modulator can be built utilizing the inherent polarization field, where the extra fabrication and processing steps are not required. Figure 1c shows the scanning electron microscopy (SEM) image of the fabricated IWM−LD. Owing to the high lateral resistance of the InGaN waveguiding layer and AlGaN electron blocking layer, the IM section and gain section were electrically separated, enabling the independent operation of the two sections. The isolation resistance between the two sections was 1.2 MΩ, which is 5 orders of magnitude higher than the series resistance for the LD.

Figure 2a shows the optical output power (L) vs injection current in the IWM−LD gain region (I_{LD}) with various reverse biases applied to the waveguide modulator (V_{IM} from 0 to −4 V). All the measurements were performed under continuous wave (CW) current injection. Without any modulation bias (V_{IM} = 0 V), the IWM−LD exhibits a threshold current (I_{th}) of 435 mA. Further increase in injection current to 500 mA at the gain region (I_{LD} = 1.15I_{th}) resulted in an optical output power of 15.9 mW under dc operation. The operating current was limited to 600 mA as the thermal rollover became significant when I_{LD} > 600 mA. With increasing $|V_{IM}|$ applied to the IM region, decreasing optical power and increasing lasing threshold current were observed in the IWM−LD device due to increasing loss. For example, the optical power of IWM−LD at I_{LD} = 500 mA was reduced to 9.3, 4.6, and 1.8 mW at V_{IM} = −2, −3, and −3.5 V, respectively. The strong V_{IM}-dependence in optical power is evident in Figure 2b, indicating the amplitude modulation effect. The modulation bias applied to the IM section controls the light output by switching the absorption from a low value to a high value. With a constant driving current (I_{LD}) of 500 mA in the gain region, the lasing was suppressed at V_{IM} = −3.5 V, which represented the off state. The IWM−LD has its maximum emission power at V_{IM} = 0 V, which is the on state. The modulation effect can be clearly observed from the emission spot in the captured photograph (see insets in Figure 2b). At I_{LD} = 500 mA, the IWM−LD exhibited a high extinction ratio ($R_{on/off} = P_{ON}/P_{OFF}$) of 8.8 (9.4 dB) with a relatively small bias of 0/−3.5 V, compared to approximately 7 V required in c-plane modulators.[14] Our device exhibits a high modulation efficiency ($R_{on/off}/\Delta V$) of 2.68 dB/V, which is more than twice the value of that in c-plane modulators (approximately 1.11 dB/V).[14]

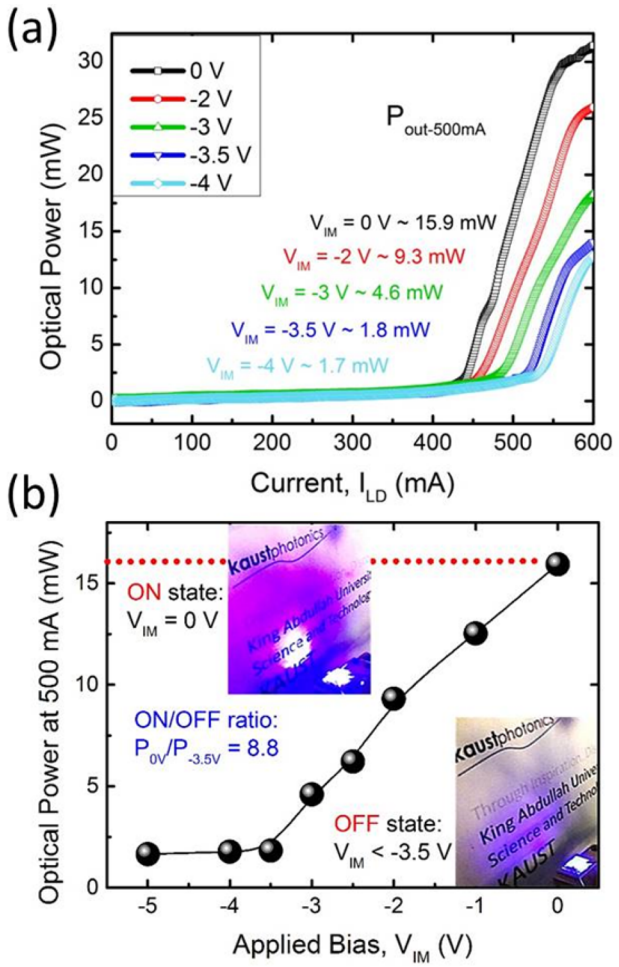

Figure 2. (a) Output power vs injection current (L−I) relations of IWM−LD with varying bias voltage applied to the IM section. The light output power at I_{LD} = 500 mA is indicated. (b) Light output power at an injection of 500 mA in the gain region ($P_{out\text{-}500\ mA}$) as a function of the applied modulation bias in the IM section (V_{IM}). Insets: Photographs of the fabricated IWM−LD operating in on and off states.

To study the EA modulation effect in the IWM−LD, the changes in absorption ($\Delta\alpha$) of semipolar InGaN/GaN QWs were obtained from the electrotransmission measurements with different modulation bias voltages applied to the QW. The spectra of absorption changes shown in Figure 3a were derived based on the transmission spectrum at zero modulation bias, according to the relationship

$$\Delta\alpha = -\frac{1}{d}\ln(P_{V_{IM}}/P_{0V})$$

where d is the total thickness of the InGaN QW layers. $P_{V_{IM}}$ refers to the transmitted optical power when modulation bias is applied to the device, and P_{0V} refers to the transmitted optical power at zero modulation bias. The external-field-induced absorption changes occur for photon energies near the transition energy of QWs within the space charge region of the p−i−n junction. Because the active layer for our device consists of InGaN QWs embedded within GaN barriers, the EA signature for the InGaN layers, with a total thickness (d) of 14.4 nm, can be observed separately at 448 nm. The absorption of the InGaN QWs can be strongly modulated around the lasing wavelength by the applied external field. With increasing modulation bias $|V_{IM}|$ from −1 V to −6 V, a broadening and red-shift of the absorption edge can be identified in a semipolar $(20\bar{2}1)$ plane InGaN/GaN waveguide modulator. This trend, in which the increasing modulation bias leads to a growing internal field within the entire space charge region, is similar to the behavior of AlGaAs/GaAs-based heterostructures, which do not present an internal piezoelectric field.[23] With increasing $|V_{IM}|$, the peak in the absorption change spectrum shifts from 441 nm (V_{IM} = −1 V) to 446 nm (V_{IM} = −6 V), and the absorption change at the lasing wavelength (λ = 448 nm) increases from 200 cm^{-1} (V_{IM} = −1 V) to 3200 cm^{-1} (V_{IM} = −6 V), which is shown in the inset of Figure 3a. The linear increase of $\Delta\alpha$ is identified at $|V_{IM}|$ > 2 V, suggesting the fully compensated piezoelectric field in the QW, which will be discussed in detail later. Our device shows efficient modulating characteristics from the bias-induced $\Delta\alpha$ rate of ∼600 cm^{-1}/V,

DOI: 10.1021/acsphotonics.5b00599
ACS Photonics 2016, 3, 262−268

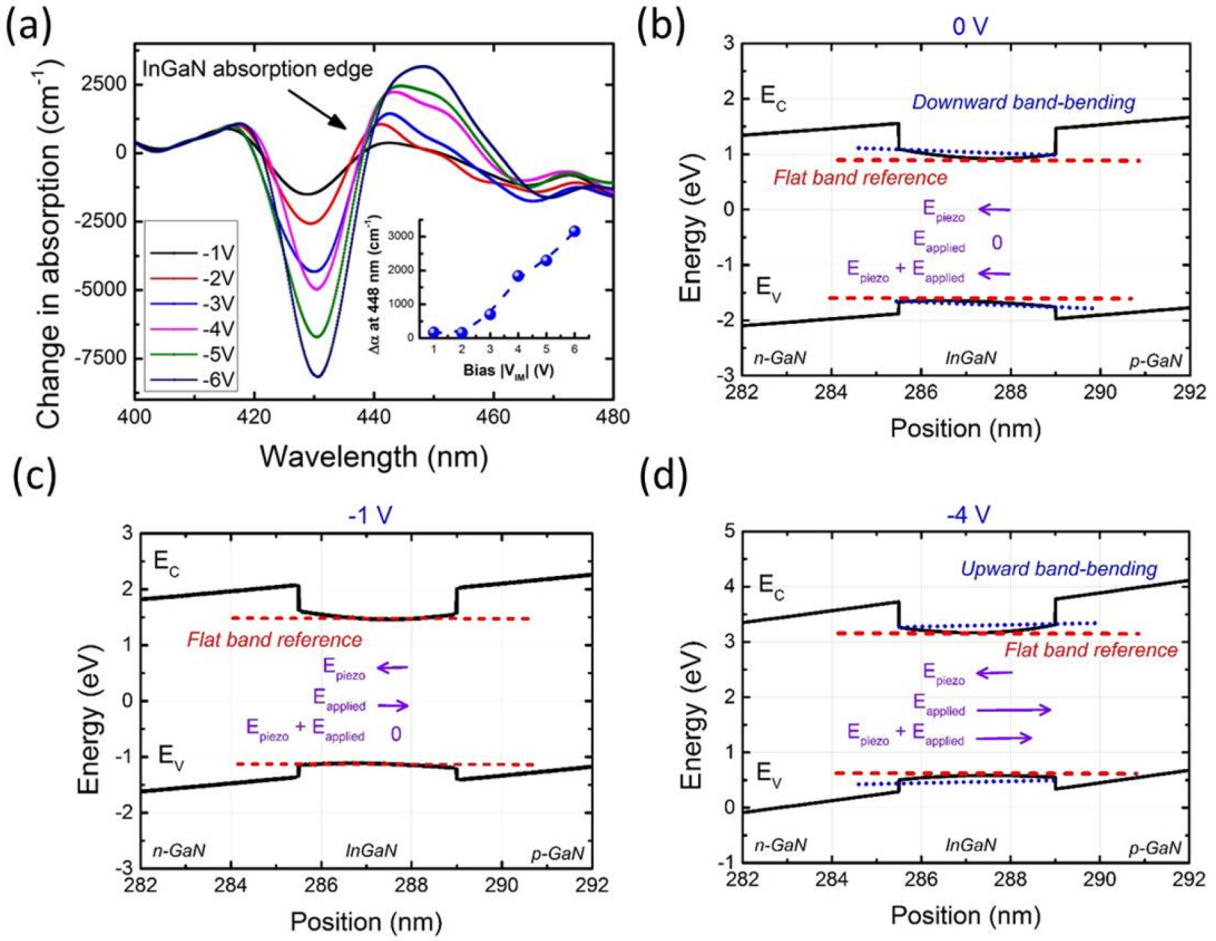

Figure 3. (a) Measured change in absorption versus wavelength in semipolar $(20\bar{2}1)$ InGaN/GaN QWs under applied reverse bias (V_{IM}) from −1 to −6 V with respect to the absorption at zero bias. Inset: Change in absorption ($\Delta\alpha$) vs modulation bias ($|V_{IM}|$) at 448 nm. (b−d) Simulated band diagram of semipolar $(20\bar{2}1)$ InGaN/GaN QWs in equilibrium showing downward band-bending (b), a flat band under reverse bias of −1 V (c), and upward band-bending at −4 V (d). The directions of the piezoelectric field (E_{piezo}), the modulation-bias-induced field ($E_{applied}$), and the combination of the fields (E_{piezo} + $E_{applied}$) are labeled. The dashed line in panel (a) shows the general trend, and the dotted lines in panels (b)−(d) serve to guide the eyes.

compared to that of ∼250 cm^{-1}/V in a *c*-plane QW structure.[24] The monotonic increase in the absorption change and red-shifting of the absorption edge are attributed to the external-field-induced QCSE, which is utilized to modulate the absorption in IWM−LDs, as shown in Figure 2.

In *c*-plane InGaN/GaN QWs, there exists a strong piezoelectric field (approximately 3.1 MV/cm in an $In_{0.2}Ga_{0.8}N$ layer)[25] due to the large total polarization discontinuity (as high as 0.03 C/m^2 in an $In_{0.2}Ga_{0.8}N$ layer).[26] Moreover, the directions of the piezoelectric field and the p−n junction built-in field in *c*-plane InGaN/GaN QWs are opposite. As a result, when a reverse modulation bias is applied to the QW grown on *c*-plane GaN, it will compensate the piezoelectric field in the InGaN QWs before introducing a net electric field in the direction of the built-in field of the QWs. Therefore, the applied modulation bias will first reverse the piezoelectric-field-induced QCSE effect, leading to a blue-shifting and narrowing of the absorption edge. Only when the applied modulation-bias-induced external field exceeds the piezoelectric field can the effect of broadening and red-shifting of the absorption edge be achieved. For typical *c*-plane InGaN-based QWs, an additional bias voltage of larger than 10 V is required to create an external field to compensate for the piezoelectric field.[27] The modulation voltage required for the semipolar $(20\bar{2}1)$ InGaN/GaN QW-based IWM−LD is, however, considerably smaller due to the significantly reduced piezoelectric field compared to the QWs grown on a polar *c*-plane. To further understand the external-field-induced effects, we performed a simulation study to investigate the band-bending in semipolar $(20\bar{2}1)$ InGaN/GaN QWs using SiLENSe.[28] The SILENSe package from the STR Group uses a 1D Schrödinger−Poisson solver with a drift-diffusion model and accounts for the effects of polarization and strain for arbitrary crystallography orientations. Figure 3b shows the band diagram in equilibrium, where a band-bending can be identified owing to the piezoelectric field (E_{piezo}). When a negative bias is applied, the modulation-bias-induced field ($E_{applied}$) will first compensate the piezoelectric field to reach the flat-band condition (E_{piezo} + $E_{applied}$ = 0). In semipolar $(20\bar{2}1)$ InGaN/GaN QWs, a flat band is observed in the band diagram of the QWs under a reverse bias of −1 V, as shown in Figure 3c, indicating a much smaller external field required to compensate E_{piezo}. With increasing reverse bias to −4 V, $E_{applied}$ exceeds E_{piezo}, resulting in a band-bending of the opposite direction to the equilibrium condition, which is identified in the band diagram of the QWs shown in Figure 3d. As a result, the

DOI: 10.1021/acsphotonics.5b00599
ACS Photonics 2016, 3, 262−268

introduction of an external-field-induced quantum-confined Stark effect leads to a major change in absorption at the lasing wavelength, which can be as large as 1800 cm^{-1} with a small modulation bias of −4 V according to the measurement shown in Figure 3a. The theoretical modeling confirmed the fact that a considerably small modulation voltage is expected in blue-green-emitting IWM−LDs based on semipolar InGaN/GaN QWs, leading to high modulation efficiency and low power consumption. Although the above investigation is performed on semipolar $(20\bar{2}1)$ InGaN/GaN QWs, similar behavior is expected in other semipolar plane QWs, such as $(20\bar{2}1)$, which is favorable for green light emitters.[19]

We performed the photocurrent measurements to further investigate the external-field-dependent optical absorption response in semipolar $(20\bar{2}1)$ InGaN/GaN QWs. Figure 4a

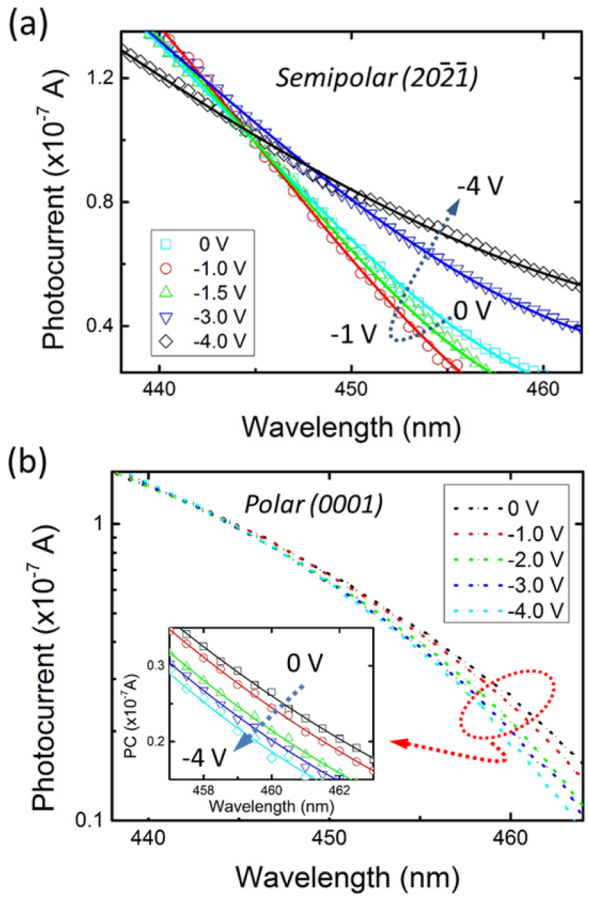

Figure 4. Photocurrent spectra of (a) semipolar $(20\bar{2}1)$ and (b) *c*-plane (0001) InGaN/GaN quantum well modulators with an applied dc bias of −4 to 0 V.

illustrates the photocurrent spectrum collected around the absorption edge of the device at room temperature. For comparison purposes, we also measured the photocurrent spectrum from *c*-plane InGaN/GaN QWs with a similar transition energy, shown in Figure 4b. As expected, the polar QW exhibits a monotonic blue-shifting absorption edge with an increasing applied electric field due to the reversed QCSE with V_{IM} from 0 to −4 V. With regard to the semipolar QW, similar blue-shifting was observed when a small negative bias was applied (0 to −1 V). However, the absorption edge of the semipolar QW shows a red-shifting trend when an increasing negative bias (>2 V) is applied, which is similar to the behavior of GaAs-based QWs.[29] The red-shifting clearly indicates the occurrence of a QCSE-induced red-shift in the absorption edge. This is in contrast to the conventional *c*-plane InGaN-based modulator structure, where a blue-shifting of absorption edge is observed, leading to low modulation efficiency.[24] The change is due to the applied external field on the IM canceling the built-in polarization-induced electric fields in the active region and thus manifesting itself as in conventional GaAs-based materials. Due to a reduced piezoelectric field in semipolar QWs, the significant shifting of absorption edges in the IM region in response to modulation bias is effective in modulating the optical output power of the IWM−LD.

For a proof-of-concept demonstration of ac modulation using the proposed IWM−LD scheme, we performed a small-signal modulation measurement by applying a −10 dBm ac signal to the integrated modulator while pumping the gain region with a constant driving current (500 mA). Figure 5

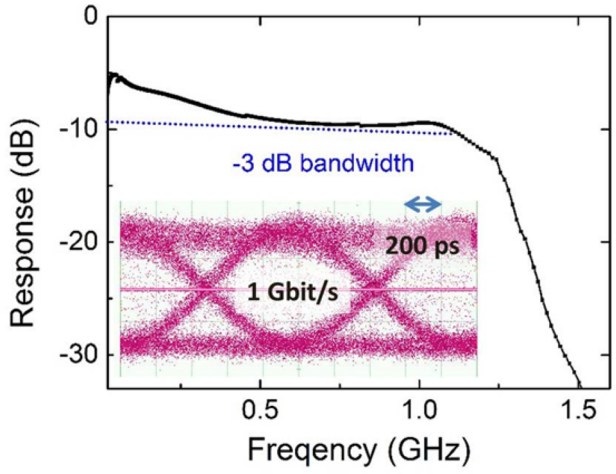

Figure 5. Small signal modulation response of IWM−LD under an injection current of 500 mA and IM bias of −3.5 V shows a −3 dB bandwidth of ∼1 GHz. Inset: Eye-diagram of 1 Gbit/s data rate based on OOK modulation on the IWM−LD device.

illustrates the frequency response of the tested IWM−LD, in which a −3 dB bandwidth of approximately 1 GHz was measured with $|V_{IM}|$ = 3.5 V. The maximum bandwidth of the IWM−LD is expected to exceed 1 GHz due to the 1 GHz bandwidth limitation of the photodetector used in the measurement setup. Subsequently, a pseudorandom binary sequence (PRBS 2^{10}-1) NRZ-OOK data stream was used to modulate the IWM−LD, and the eye diagram showing data rate at 1 Gbit/s can be found in the inset of Figure 5. The open eye observed from the figure confirms the potential of utilizing an integrated waveguide modulator for high-speed VLC applications. Higher data rates could be achieved by further optimization of the system and employing complex modulation schemes, such as OFDM. Nevertheless, our demonstration proves the feasibility of using IWM−LD for data transmission.

CONCLUSIONS

We demonstrated the monolithic integration of a waveguide EA modulator with a laser diode and measured the dc and ac modulation characteristics of the device, which is grown on a $(20\bar{2}1)$ plane GaN substrate. By alternating the modulation voltages at −3.5 and 0 V, the laser output power was tuned from 1.8 mW to 15.9 mW, respectively, leading to an on/off

DOI: 10.1021/acsphotonics.5b00599
ACS Photonics 2016, 3, 262−268

ratio of 9.4 dB. Our results clearly demonstrated that modulation can be achieved using a semipolar EA−modulator that consumes less power compared to *c*-plane devices. Our work discloses the physical mechanism of QCSE-induced absorption change, leading to the promising deployment of the blue-green-red electromagnetic spectrum for utilization in compact SSL−VLC devices. Moving forward, we noted that the present work is beneficial for III−V−Si integration, by combining III−N lasers and CMOS-based Si photodetectors. Thus, our investigation into GaN-based IWM−LD at 448 nm has the potential for further implementation in high-speed optical interconnects and photonic integrated circuits.[30−32]

AUTHOR INFORMATION

Corresponding Author

*E-mail: boon.ooi@kaust.edu.sa.

Notes

The authors declare no competing financial interest.

ACKNOWLEDGMENTS

The authors acknowledge funding support from KAUST baseline funding, grant no. BAS/1/1614-01-01, King Abdulaziz City for Science and Technology (KACST) Technology Innovation Center (TIC) for Solid State Lighting, grant no. KACST TIC R2-FP-008, and KACST-KAUST-UCSB Solid-State Lighting Program.

REFERENCES

(1) Waltereit, P.; Brandt, O.; Trampert, A.; Grahn, H. T.; Menniger, J.; Ramsteiner, M.; Reiche, M.; Ploog, K. H. Nitride semiconductors free of electrostatic fields for efficient white light-emitting diodes. *Nature* **2000**, *406*, 865−868.

(2) Pimputkar, S.; Speck, J. S.; DenBaars, S. P.; Nakamura, S. Prospects for LED lighting. *Nat. Photonics* **2009**, *3*, 180−182.

(3) Denault, K. A.; Cantore, M.; Nakamura, S.; DenBaars, S. P.; Seshadri, R. Efficient and stable laser-driven white lighting. *AIP Adv.* **2013**, *3*, 072107.

(4) Lin, G.-B.; Schubert, E. F.; Cho, J.; Park, J. H.; Kim, J. K. Onset of the Efficiency Droop in GaInN Quantum Well Light-Emitting Diodes under Photoluminescence and Electroluminescence Excitation. *ACS Photonics* **2015**, *2*, 1013−1018.

(5) Tsonev, D.; Videv, S.; Haas, H. Towards a 100 Gb/s visible light wireless access network. *Opt. Express* **2015**, *23*, 1627−1637.

(6) Watson, S.; Tan, M. M.; Najda, S. P.; Perlin, P.; Leszczynski, M.; Targowski, G.; Grzanka, S.; Kelly, A. E. Visible light communications using a directly modulated 422 nm GaN laser diode. *Opt. Lett.* **2013**, *38*, 3792−3794.

(7) Chi, Y.-C.; Hsieh, D.-H.; Tsai, C.-T.; Chen, H.-Y.; Kuo, H.-C.; Lin, G.-R. 450-nm GaN laser diode enables high-speed visible light communication with 9-Gbps QAM-OFDM. *Opt. Express* **2015**, *23*, 13051−13059.

(8) Lee, C.; Shen, C.; Oubei, H. M.; Cantore, M.; Janjua, B.; Ng, T. K.; Farrell, R. M.; El-Desouki, M. M.; Speck, J. S.; Nakamura, S.; Ooi, B. S.; DenBaars, S. P. 2 Gbit/s data transmission from an unfiltered laser-based phosphor-converted white lighting communication system. *Opt. Express* **2015**, *23*, 29779−29787.

(9) Yu, R.; Pruneri, V.; García de Abajo, F. J. Resonant Visible Light Modulation with Graphene. *ACS Photonics* **2015**, *2*, 550−558.

(10) Abe, T.; Yamane, N.; Nishiguchi, T.; Kozeni, H.; Yoshida, T.; Adachi, M.; Kasada, H.; Ando, K. Demonstration of practical blue waveguide stark-effect modulators of ZnSe/ZnMgSSe asymmetric coupled quantum wells. *J. Korean Phys. Soc.* **2008**, *53*, 94−97.

(11) Ozel, T.; Sari, E.; Nizamoglu, S.; Demir, H. V. Violet to deep-ultraviolet InGaN/GaN and GaN/AlGaN quantum structures for UV electroabsorption modulators. *J. Appl. Phys.* **2007**, *102*, 113101.

(12) Sari, E.; Ozel, T.; Koc, A.; Ju, J. W.; Ahn, H. K.; Lee, I. H.; Baek, J. H.; Demir, H. V. Comparative study of electroabsorption in InGaN/GaN quantum zigzag heterostructures with polarization-induced electric fields. *Appl. Phys. Lett.* **2008**, *92*, 201105.

(13) Kao, C. K.; Bhattacharyya, A.; Thomidis, C.; Paiella, R.; Moustakas, T. D. Electroabsorption modulators based on bulk GaN films and GaN/AlGaN multiple quantum wells. *J. Appl. Phys.* **2011**, *109*, 083102.

(14) Kneissl, M.; Paoli, T. L.; Kiesel, P.; Treat, D. W.; Teepe, M.; Miyashita, N.; Johnson, N. M. Two-section InGaN multiple-quantum-well laser diode with integrated electroabsorption modulator. *Appl. Phys. Lett.* **2002**, *80*, 3283−3285.

(15) Dummer, M. M.; Raring, J. R.; Klamkin, J.; Tauke-Pedretti, A.; Coldren, L. A. Selectively-undercut traveling-wave electroabsorption modulators incorporating a p-InGaAs contact layer. *Opt. Express* **2008**, *16*, 20388−20394.

(16) Schmiedel, G.; Kiesel, P.; Dohler, G. H.; Greger, E.; Gulden, K. H.; Schweizer, H. P.; Moser, M. Electroabsorption in ordered and disordered GaInP. *J. Appl. Phys.* **1997**, *81*, 1008−1010.

(17) Zhao, Y. J.; Yan, Q. M.; Feezell, D.; Fujito, K.; Van de Walle, C. G.; Speck, J. S.; DenBaars, S. P.; Nakamura, S. Optical polarization characteristics of semipolar $(30\bar{3}1)$ and $(30\bar{3}\bar{1})$ InGaN/GaN light-emitting diodes. *Opt. Express* **2013**, *21*, A53−A59.

(18) Pourhashemi, A.; Farrell, R. M.; Cohen, D. A.; Speck, J. S.; DenBaars, S. P.; Nakamura, S. High-power blue laser diodes with indium tin oxide cladding on semipolar $(20\bar{2}1)$ GaN substrates. *Appl. Phys. Lett.* **2015**, *106*, 111105.

(19) Adachi, M. InGaN based green laser diodes on semipolar GaN substrate. *Jpn. J. Appl. Phys.* **2014**, *53*, 100207.

(20) Zhao, Y. J.; Yan, Q. M.; Huang, C. Y.; Huang, S. C.; Hsu, P. S.; Tanaka, S.; Pan, C. C.; Kawaguchi, Y.; Fujito, K.; Van de Walle, C. G.; Speck, J. S.; DenBaars, S. P.; Nakamura, S.; Feezell, D. Indium incorporation and emission properties of nonpolar and semipolar InGaN quantum wells. *Appl. Phys. Lett.* **2012**, *100*, 201108.

(21) Feezell, D. F.; Speck, J. S.; DenBaars, S. P.; Nakamura, S. Semipolar $(20\bar{2}1)$ InGaN/GaN Light-Emitting Diodes for High-Efficiency Solid-State Lighting. *J. Disp. Technol.* **2013**, *9*, 190−198.

(22) Lammert, R. M.; Smith, G. M.; Hughes, J. S.; Osowski, M. L.; Jones, A. M.; Coleman, J. J. MQW wavelength-tunable DBR lasers with monolithically integrated external cavity electroabsorption modulators with low-driving voltages fabricated by selective-area MOCVD. *IEEE Photonics Technol. Lett.* **1996**, *8*, 797−799.

(23) Renner, F.; Kiesel, P.; Dohler, G. H.; Kneissl, M.; Van de Walle, C. G.; Johnson, N. M. Quantitative analysis of the polarization fields and absorption changes in InGaN/GaN quantum wells with electroabsorption spectroscopy. *Appl. Phys. Lett.* **2002**, *81*, 490−492.

(24) Sari, E.; Nizamoglu, S.; Ozel, T.; Demir, H. V. Blue quantum electroabsorption modulators based on reversed quantum confined Stark effect with blueshift. *Appl. Phys. Lett.* **2007**, *90*, 011101.

(25) Turchinovich, D.; Jepsen, P. U.; Monozon, B. S.; Koch, M.; Lahmann, S.; Rossow, U.; Hangleiter, A. Ultrafast polarization dynamics in biased quantum wells under strong femtosecond optical excitation. *Phys. Rev. B: Condens. Matter Mater. Phys.* **2003**, *68*, 241307.

(26) Feezell, D. F.; Speck, J. S.; DenBaars, S. P.; Nakamura, S. Semipolar $(20\bar{2}1)$ InGaN/GaN Light-Emitting Diodes for High-Efficiency Solid-State Lighting. *J. Disp. Technol.* **2013**, *9*, 190−198.

(27) Brown, I. H.; Pope, I. A.; Smowton, P. M.; Blood, P.; Thomson, J. D.; Chow, W. W.; Bour, D. P.; Kneissl, M. Determination of the piezoelectric field in InGaN quantum wells. *Appl. Phys. Lett.* **2005**, *86*, 131108.

(28) Huang, C.-Y.; Hardy, M. T.; Fujito, K.; Feezell, D. F.; Speck, J. S.; DenBaars, S. P.; Nakamura, S. Demonstration of 505 nm laser diodes using wavelength-stable semipolar $(20\bar{2}1)$ InGaN/GaN quantum wells. *Appl. Phys. Lett.* **2011**, *99*, 241115.

(29) Krol, M. F.; Leavitt, R. P.; Pham, J. T.; Mcginnis, B. P.; Peyghambarian, N. Enhanced Electroabsorption in Selectively Doped (Ga,In)As/Al,In)As Asymmetric Double-Quantum Wells. *Appl. Phys. Lett.* **1995**, *66*, 3045−3047.

DOI: 10.1021/acsphotonics.5b00599
ACS Photonics 2016, 3, 262−268

(30) Cho, S. Y.; Seo, S. W.; Brooke, M. A.; Jokerst, N. M. Integrated detectors for embedded optical interconnections on electrical boards, modules, and integrated circuits. *IEEE J. Sel. Top. Quantum Electron.* **2002**, *8*, 1427−1434.
(31) Tchernycheva, M.; Messanvi, A.; Bugallo, A. D.; Jacopin, G.; Lavenus, P.; Rigutti, L.; Zhang, H.; Halioua, Y.; Julien, F. H.; Eymery, J.; Durand, C. Integrated Photonic Platform Based on InGaN/GaN Nanowire Emitters and Detectors. *Nano Lett.* **2014**, *14*, 3515−3520.
(32) Haurylau, M.; Chen, G. Q.; Chen, H.; Zhang, J. D.; Nelson, N. A.; Albonesi, D. H.; Friedman, E. G.; Fauchet, P. M. On-chip optical interconnect roadmap: Challenges and critical directions. *IEEE J. Sel. Top. Quantum Electron.* **2006**, *12*, 1699−1705.

DOI: 10.1021/acsphotonics.5b00599
ACS Photonics 2016, 3, 262−268